

ELECTRONIC SUPPORTING INFORMATION

Interference of citrate-stabilized gold nanoparticles on β 2-microglobulin oligomeric association

Cristina Cantarutti,^a Gijo Raj,^b Federico Fogolari,^{c,d} Sofia Giorgetti,^e Alessandra Corazza,^{a,c} Vittorio Bellotti,^{e,f} Panče Naumov^b and Gennaro Esposito^{*b,c,d}

^a *DAME, Università di Udine, P.le Kolbe 4, 33100 Udine, Italy.*

^b *Science and Math Division, New York University Abu Dhabi, PO Box 129188, Abu Dhabi, UAE.*

^c *INBB, Viale Medaglie d'Oro 305, 00136 Roma, Italy.*

^d *DMIF, Università di Udine, Viale delle Scienze, 33100 Udine, Italy.*

^e *Dipartimento di Medicina Molecolare, Università di Pavia, Via Taramelli 3, 27100 Pavia, Italy*

^f *Division of Medicine, University College of London, London NW3 2PF, UK.*

Materials and Methods

All reagents were used as received, without further purification. Tetrachloroauric(III) acid trihydrate, trisodium citrate dihydrate, sodium borohydride and HEPES were purchased from Sigma-Aldrich. Wild-type and D76N β 2m ^{15}N -uniformly-labeled came from overexpression in transformed *E. coli* BL21DE3 strains, according to the procedures previously described.^{1,2} The lyophilized proteins were dissolved in 50 mM HEPES buffer at pH 7.

Cit-AuNP synthesis and characterization

All glassware used in nanoparticle synthesis was washed with *aqua regia* and dried in oven before use. To prepare citrate-stabilized gold nanoparticles of 7.5 nm, a standard cold synthesis using NaBH_4 as gold reducing agent was employed, as reported before.³ Cit-AuNP were characterized by UV-Vis spectroscopy and transmission electron microscopy (TEM). The concentration of reduced gold (Au^0) was determined by the UV-Vis absorbance of the colloidal solution at 400 nm⁴ and used to estimate the molar concentration of nanoparticles considering the average number of gold atoms per nanoparticle (N) expressed by the following equation:⁵

$$N = \frac{\pi \rho d^3}{6 M} = 30.89602d^3 \quad (1)$$

where d is the nanoparticles diameter (nm), ρ is the density for face-centered cubic gold (19.3 g/cm^3) and M stands for atomic weight of gold (197 g/mol). The analysis of the nanoparticle surface plasmon resonance (SPR) in the UV-Vis spectrum (Fig. S1a) was performed with a JASCO UV-530 spectrophotometer by acquiring a spectrum in the range from 400 to 600 nm with a band-width of 2.0 nm, a data pitch of 0.2 nm and a speed of 40 nm/min. TEM images (Fig. S1b) were recorded using a Tecnai G2. 5 μL of Cit-AuNP solution were dropped on a Cu 400-mesh TEM grid and left at room temperature for 3 hours to allow for solvent evaporation. The size distribution was calculated by measuring a minimum of 200 particles using the ImageJ software.

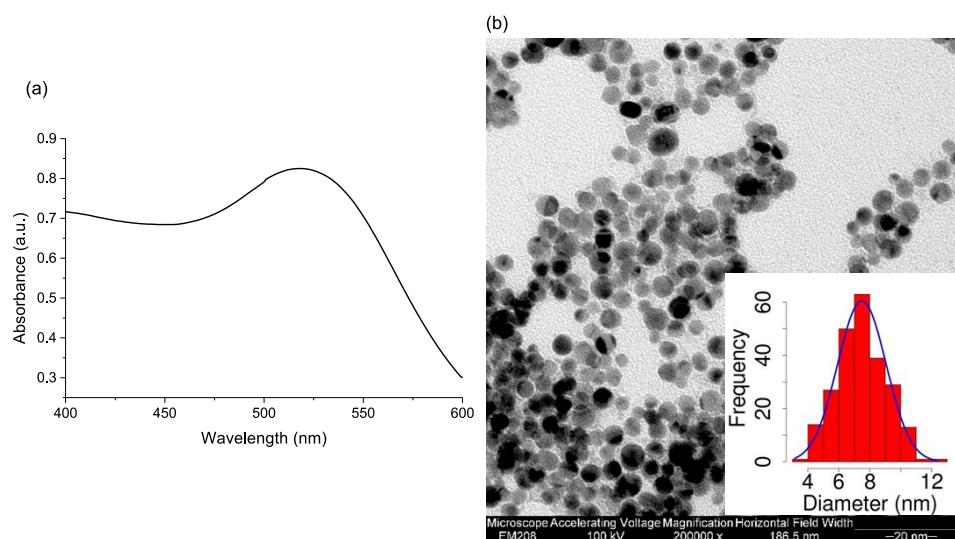


Fig. S1 a) Absorption spectrum and b) TEM micrograph of synthesized Cit-AuNP. The insert presents the size distribution histogram (Average diameter = 7.5 ± 1.0 nm).

NMR spectroscopy

NMR samples were prepared by dissolving lyophilized ^{15}N -labeled wild-type and D76N $\beta 2\text{m}$ in 50 mM HEPES, 1.5 mM sodium citrate, pH 7 and 5% D_2O . For each variant two samples were prepared at concentrations of 4 and 17 μM . NMR spectra were collected at 14.0 T, on the Bruker Avance III NMR facility of the Core Technology Platform at New York University Abu Dhabi. The spectrometer, equipped with cryoprobe and z-axis gradient unit, operated at 600.13 and 60.85 MHz to observe ^1H and ^{15}N , respectively. 2D ^{15}N - ^1H HSQC⁶ spectra were recorded over spectral widths of 40 ppm (^{15}N , t_1) and 15 ppm (^1H , t_2), and digitized over 128 and 2048 points, respectively. For each t_1 dimension point, 128 or 64 scans were accumulated and quadrature in the same dimension was accomplished by gradient-assisted coherence selection (echo-antiecho).⁷ Processing with t_1 linear prediction, apodization and zero-filling prior to Fourier transformation led to $2\text{K}\times 1\text{K}$ real spectra. Water suppression was achieved by using a flip-back pulse in the HSQC experiments.⁸ All measurements were performed at 25 $^\circ\text{C}$. The data were processed with Topspin 3.5 and analysed with Sparky. Chemical shift perturbations were calculated as $\Delta\delta$ (ppm) = $[(\Delta\delta_{\text{H}})^2 + (\Delta\delta_{\text{N}}/6.5)^2]^{1/2}$ where $\Delta\delta_{\text{H}}$ and $\Delta\delta_{\text{N}}$ are the chemical shift variations for ^1H and ^{15}N , respectively,⁹ and the relative intensities (RI) correspond to the ratio between the signal intensity in presence of Cit-AuNP and in absence of Cit-AuNP. The uncertainty related to the relative intensity ratio was calculated applying the propagation of the intensity error estimated from the signal-to-noise ratio. The experimental $\Delta\delta$ uncertainty was always $\pm 9.8\times 10^{-3}$ ppm.

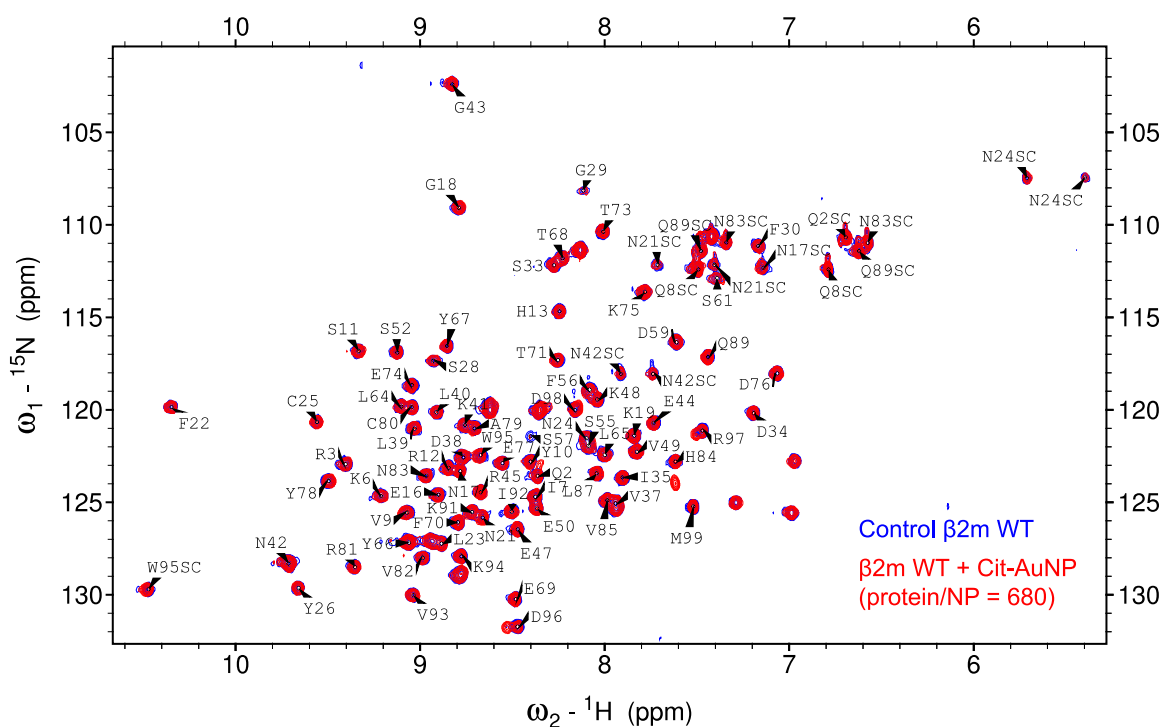


Fig. S2 Superimposition of $\beta 2\text{m}$ WT ^{15}N - ^1H HSQC spectra recorded at 600 MHz without (blue) and with (red) Cit-AuNP (protein/NP = 680). The corresponding backbone amide assignments are reported by single letter code and side chain amides are indicated with SC.

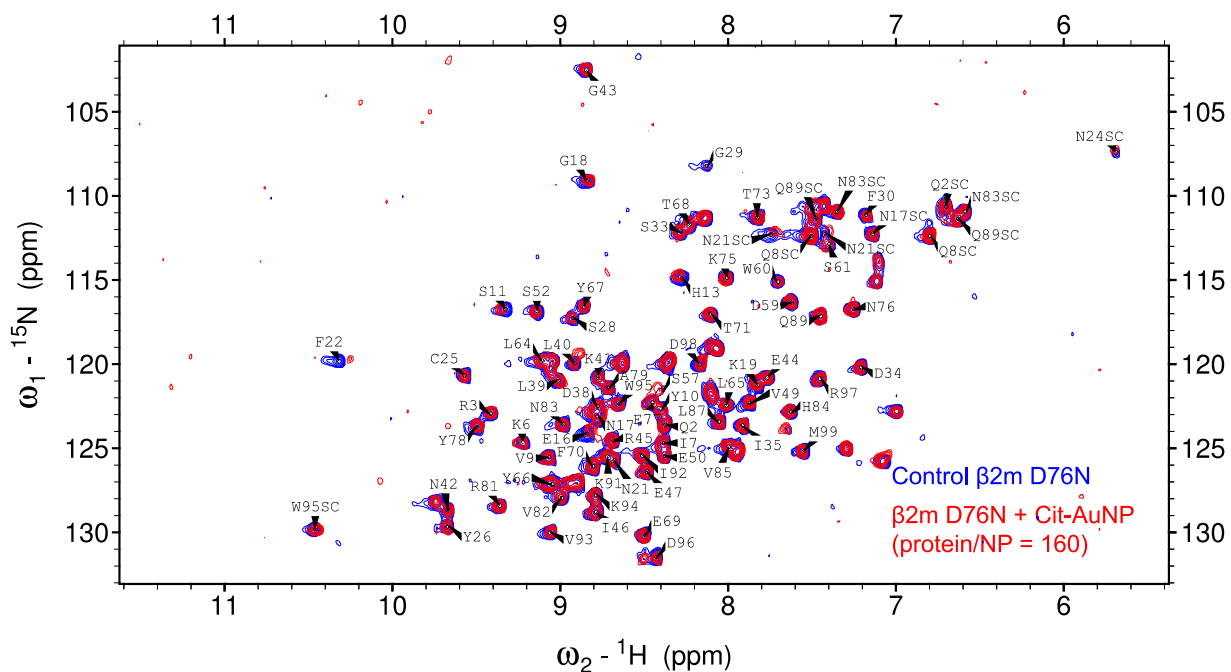


Fig. S5 Superimposition of $\beta 2m$ D76N ^{15}N - 1H HSQC spectra recorded at 600 MHz without (blue) and with (red) Cit-AuNP (protein/NP = 160). The corresponding backbone amide assignments are reported by single letter code and side chain amides are indicated with SC.

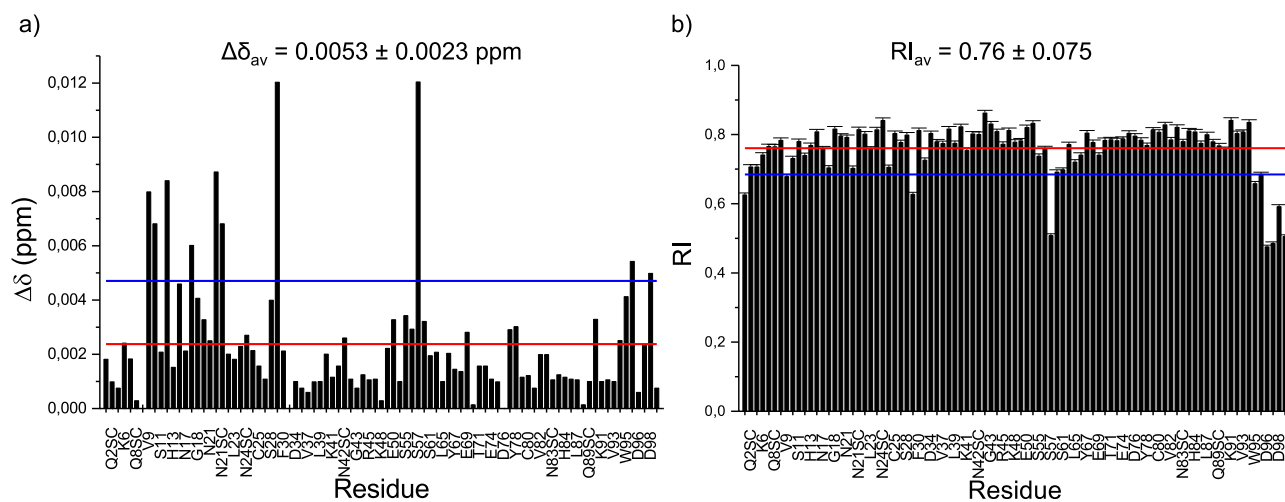


Fig. S6 a) and b) Bar plots of amide chemical shift perturbations ($\Delta\delta$) and cross-peak attenuations (RI), respectively, for $\beta 2m$ WT (protein/NP = 680). The two horizontal lines indicate the average values (red) and the displacement of one standard deviation (blue) above and below the average, respectively. To avoid graphic crowding, the abscissa labels of both panels were reported only every other two signals. Besides the observed backbone amides, also the following detected side-chain (SC) NH resonances were included in the abscissa label list, according to the primary sequence order: Q2, Q8*, N17, N21*, N24*, N42*, N83*, Q89*, W95, where the asterisk indicates the inclusion of two separate resonances for asparagine and glutamine side-chain amides. The missing labels do not include the following unobserved or non-existing backbone NH connectivities: I1, T4, P5, Q8, P14, A15, S20, V27, H31, P32, H51, D53, L54, S57, K58, F62, Y63, P72, T86, S88, P90.

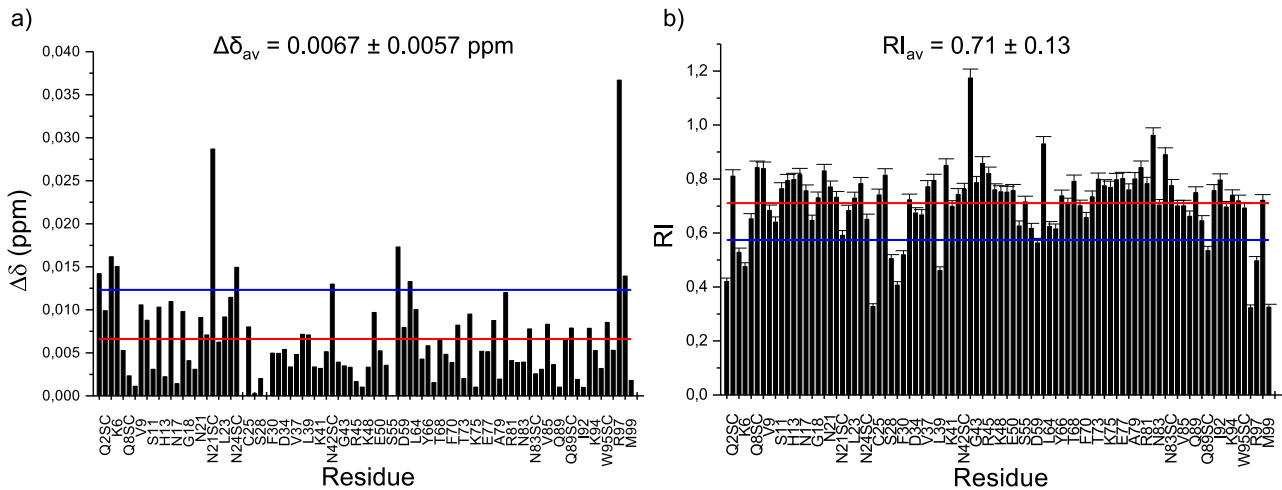


Fig. S7 a) and b) Bar plots of amide chemical shift perturbations ($\Delta\delta$) and cross-peak attenuations (RI), respectively. The two horizontal lines indicate the average values (red) and the displacement of one standard deviation (blue) above and below the average, respectively, for $\beta 2m$ WT (protein/NP = 160). To avoid graphic crowding, the abscissa labels of both panels were reported only every other two signals. Besides the observed backbone amides, also the following detected side-chain (SC) NH resonances were included in the abscissa label list, according to the primary sequence order: Q2, Q8*, N17, N21*, N24*, N42*, N83*, Q89*, W95, where the asterisk indicates the inclusion of two separate resonances for asparagine and glutamine side-chain amides. The missing labels do not include the following unobserved or non-existing backbone NH connectivities: I1, T4, P5, Q8, P14, A15, S20, V27, H31, P32, E36, H51, D53, L54, S57, K58, W60, F62, Y63, P72, T86, S88, P90.

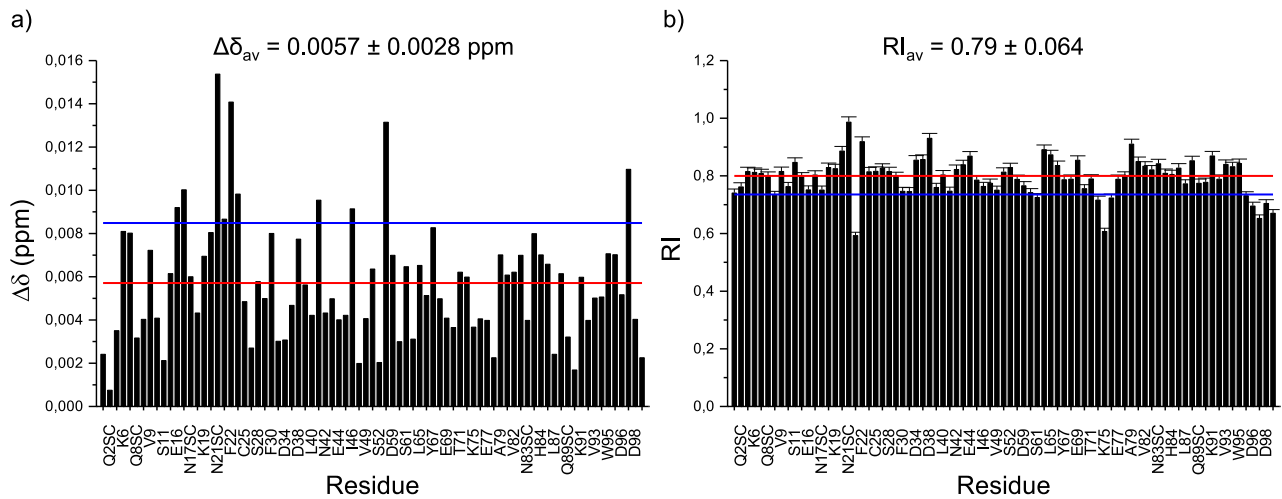


Fig. S8 a) and b) Bar plots of amide chemical shift perturbations ($\Delta\delta$) and cross-peak attenuations (RI), respectively. The two horizontal lines indicate the average values (red) and the displacement of one standard deviation (blue) above and below the average, respectively, for $\beta 2m$ D76N (protein/NP = 680). To avoid graphic crowding, the abscissa labels of both panels were reported only every other two signals. Besides the observed backbone amides, also the following detected side-chain (SC) NH resonances were included in the abscissa label list, according to the primary sequence order: Q2, Q8*, N17, N21*, N24*, N42*, N83*, Q89*, W95, where the asterisk indicates the inclusion of two separate resonances for asparagine and glutamine side-chain amides. The missing labels do not include the following unobserved or non-existing backbone NH connectivities: I1, T4, P5, Q8, R12, P14, A15, S20, L23, N24, V27, H31, P32, E36, V37, H51, D53, L54, F56, S57, K58, F62, Y63, P72, E74, C80, T86, S88, P90.

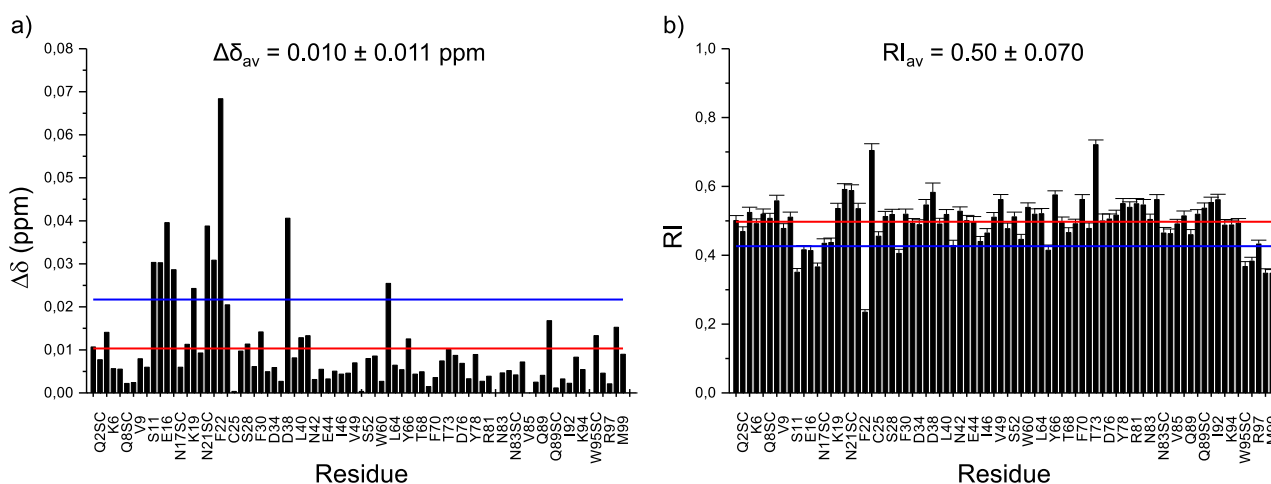


Fig. S9 a) and b) Bar plots of amide chemical shift perturbations ($\Delta\delta$) and cross-peak attenuations (RI), respectively. The two horizontal lines indicate the average values (red) and the displacement of one standard deviation (blue) above and below the average, respectively, for D76N β 2m (protein/NP = 160). To avoid graphic crowding, the abscissa labels of both panels were reported only every other two signals. Besides the observed backbone amides, also the following detected side-chain (SC) NH resonances were included in the abscissa label list, according to the primary sequence order: Q2, Q8*, N17, N21*, N24*, N42*, N83*, Q89*, W95, where the asterisk indicates the inclusion of two separate resonances for asparagine and glutamine side-chain amides. The missing labels do not include the following unobserved or non-existing backbone NH connectivities: I1, T4, P5, Q8, R12, P14, A15, S20, L23, N24, V27, H31, P32, E36, V37, H51, D53, L54, F56, S57, K58, F62, Y63, P72, E74, C80, T86, S88, P90.

Diffusion coefficients were determined by means of 2D 1H DSTEBPP (Double Stimulated Echo BiPolar Pulse) experiments.¹⁰ Protein concentration was 4 μ M in 50 mM HEPES, 1.5 mM sodium citrate, pH = 7 in 95/5 H₂O/D₂O, either in absence and in presence of Cit-AuNP. The z-axis gradient strength was varied with a squared increment ramp from 10 to 90 % of its maximum value (~ 60 G/cm) and matrices of 2048 by 40 points were collected by accumulating 512 scans per gradient increment. Water suppression was carefully adjusted by appending to the DSTEBPP sequence a pair of WATERGATE¹¹ elements in the excitation-sculpting mode.¹²

Quartz crystal microbalance with dissipation monitoring (QCMD)

QCMD experiments were performed using the QSense Analyzer instrument (Biolin Scientific, Sweden) of the Core Technology Platform at New York University Abu Dhabi. A solution of 1 μ M D76N β 2m in 50 mM HEPES, 1.5 mM sodium citrate, pH = 7, without or with 25 nM Cit-AuNP was flowed over an Au-coated QCMD sensor (model: QSX-301). Control experiments were also carried out with 25 nM Cit-AuNP alone. The solutions were drawn into the standard QSense flow module at the rate of 50 μ L/min for 5000 seconds approximately using a peristaltic pump (model: IPC, ISMATEC Germany) and tygon tubing (model: LMT-55, Saint-Gobain, France). Frequency and dissipation changes were recorded at 22°C and after any adsorption experiment, a rinsing step with the buffer solution was performed.

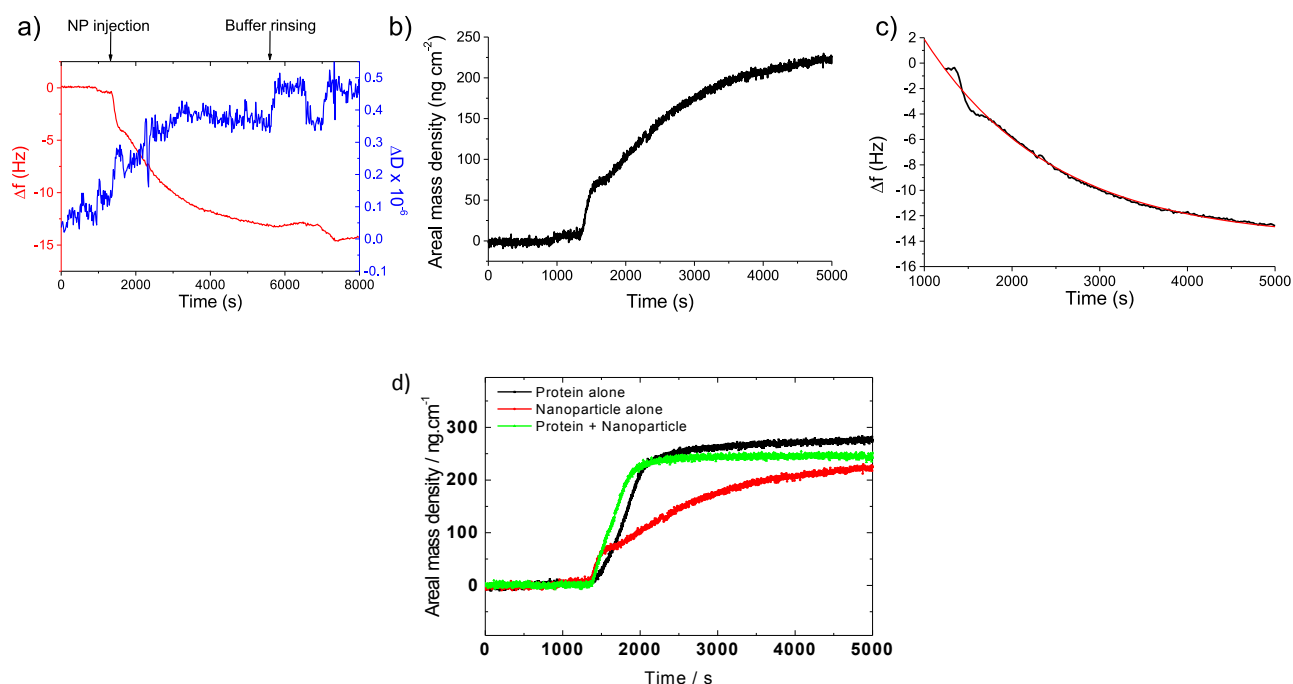


Fig. S10 a) Normalized frequency (red) and dissipation (blue) plots during adsorption onto an Au-coated QCMD sensor of Cit-AuNP control solution; b) time course of the adsorbed areal mass density as obtained by Sauerbrey equation from QCMD measurements on Cit-AuNP control solution and c) fitting of the QCMD frequency time course for Cit-AuNP control solution. The red line indicates the fitting according to Boltzmann equation (see main text); d) overlay of the time evolution of the areal mass density from the protein alone (black), protein + Cit-AuNP (green) and Cit-AuNP alone (red) reported in Fig. 4a of main text and panel b) of this figure. The slower time constant of the Cit-AuNP curve is immediately evident from the time course of the areal mass density, with the related Δf that can be fitted by a time constant parameter of 1369 ± 81 s, as shown in panel c). The corresponding fitting parameters of the protein without and with Cit-AuNP are 180 ± 4 and 163 ± 2 , respectively (Table 2 of main text). The pattern of the Cit-AuNP areal mass density depicted in panels b) and d) suggests that after a rapid initial adsorption (up to 1200 s, approximately), the subsequent Cit-AuNP deposition onto the QCMD sensor increases continuously without reaching saturation. For this reason no correction was attempted to account for the contribution of the nanoparticles on the calculated protein surface density in presence of Cit-AuNP. On the other hand, the patterns of the protein without (black curve in panel d) and with NPs (green curve in panel d) have the classical sigmoid aspect. The Cit-AuNP adsorbed areal mass approaches the values of the protein, but based on the average stoichiometry of Cit-AuNP (over 3,000 Au nuclei per nanoparticle, with a molar mass beyond 2.5×10^3 kDa), the surface coverage is only 3.6% of the total occupancy expected for spheres with 7.5 nm diameter, assuming a filling factor of 0.65. This is in line with the large energy dissipation of the Cit-AuNP layer which is comparable to the dissipation of the protein in presence of nanoparticles. The Cit-AuNP adsorption parameters at saturation are compared to the corresponding values of the protein solution in Table S1.

Table S1. QCMD adsorption parameters at saturation, corresponding percentage variation after rinsing and associated surface density values.

Sample	Δf_{sat} (Hz)	ΔD_{sat} ($\times 10^{-6}$)	$\Delta f_{rinsing}$ (%)	monomers/cm ²
D76N β 2m	-15.7	0.16	2.5 %	14.5×10^{12}
D76N β 2m + Cit-AuNP	-13.9	0.39	9.3 %	12.7×10^{12}
Cit-AuNP	-12.8	0.36	12.5%	0.053×10^{12}

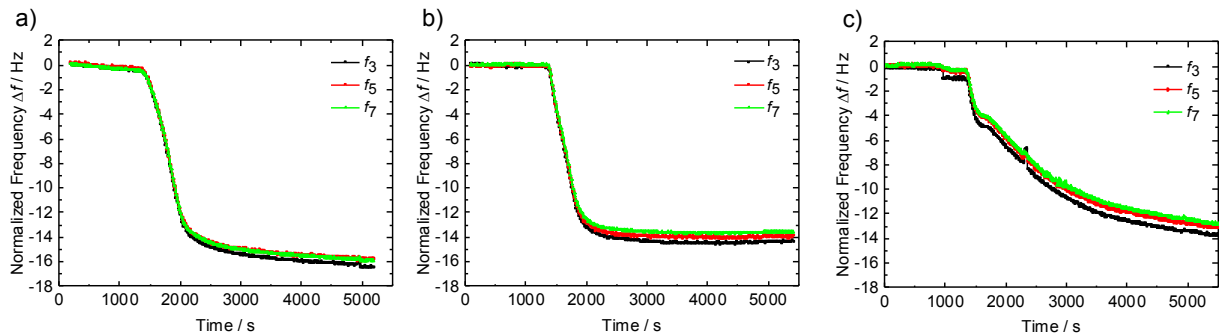


Fig. S11 Superimposition of different overtones ($n = 3, 5, 7$) of the fundamental resonance frequency changes for a) D76N β 2m alone, b) D76N β 2m + Cit-AuNP, c) Cit-AuNP alone. The different overtones of the QCMD Δf evolution nearly overlap uniformly in panel a), indicating that the protein forms a rigid layer on the sensor surface in absence of Cit-AuNP. This is no longer true in panels b) and c), i.e. for D76N β 2m+Cit-AuNP and Cit-AuNP alone, respectively. Here the overtones of the fundamental resonance frequencies are clearly separated and do not overlap. Such behavior is common to soft viscoelastic layers. Though the spread of the different overtones of Δf is visible in both panels b) and c), the patterns of Cit-AuNP alone and protein+Cit-AuNP samples are quite different. Therefore the viscoelastic properties of the Cit-AuNP are distinct from the corresponding properties of the protein+Cit-AuNP system.

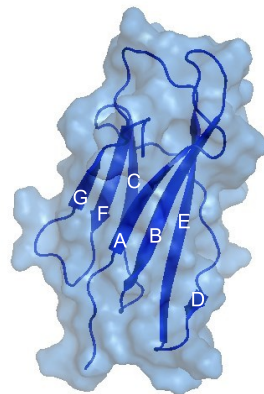


Fig. S12 Cartoon of β 2m structure. β -strand naming is also indicated. β 2m (11.862 kDa) is a globular protein whose three-dimensional structure can be assimilated to a cylindroid with longitudinal and transverse axes of 4.3-3.8 and 2.5-2.0 nm, respectively.¹³

References

- 1 S. Valleix, J. D. Gillmore, F. Bridoux, P. P. Mangione, A. Dogan, B. Nedelec, M. Boimard, G. Touchard, J.-M. Goujon, C. Lacombe, P. Lozeron, D. Adams, C. Lacroix, T. Maisonobe, V. Planté-Bordeneuve, J. A. Vrana, J. D. Theis, S. Giorgetti, R. Porcari, S. Ricagno, M. Bolognesi, M. Stoppini, M. Delpech, M. B. Pepys, P. N. Hawkins and V. Bellotti, *N. Engl. J. Med.*, 2012, **366**, 2276–2283.

- 2 G. Verdone, A. Corazza, P. Viglino, F. Pettirossi, S. Giorgetti, P. Mangione, A. Andreola, M. Stoppini, V. Bellotti and G. Esposito, *Protein Sci. Publ. Protein Soc.*, 2002, **11**, 487–499.
- 3 C. Cantarutti, S. Raimondi, G. Brancolini, A. Corazza, S. Giorgetti, M. Ballico, S. Zanini, G. Palmisano, P. Bertocin, L. Marchese, P. P. Mangione, V. Bellotti, S. Corni, F. Fogolari and G. Esposito, *Nanoscale*, 2017, **9**, 3941–3951.
- 4 T. Hendel, M. Wuthschick, F. Kettemann, A. Birnbaum, K. Rademann and J. Polte, *Anal. Chem.*, 2014, **86**, 11115–11124.
- 5 X. Liu, M. Atwater, J. Wang and Q. Huo, *Colloids Surf. B Biointerfaces*, 2007, **58**, 3–7.
- 6 G. Bodenhausen and D. J. Ruben, *Chem. Phys. Lett.*, 1980, **69**, 185–189.
- 7 J. Keeler, R. T. Clowes, A. L. Davis and E. D. Laue, *Methods Enzymol.*, 1994, **239**, 145–207.
- 8 S. Grzesiek and A. Bax, *J. Am. Chem. Soc.*, 1993, **115**, 12593–12594.
- 9 F. A. A. Mulder, D. Schipper, R. Bott and R. Boelens, *J. Mol. Biol.*, 1999, **292**, 111–123.
- 10 K. F. Morris and C. S. Johnson, *J. Am. Chem. Soc.*, 1992, **114**, 3139–3141.
- 11 M. Piotto, V. Saudek and V. Sklenár, *J. Biomol. NMR*, 1992, **2**, 661–665.
- 12 T. L. Hwang and A. J. Shaka, *J. Magn. Reson. A*, 1995, **112**, 275–279.
- 13 J. W. Becker and G. N. Reeke, *Proc. Natl. Acad. Sci. U. S. A.*, 1985, **82**, 4225–4229.